Applied Catalysis B: Environmental 97 (2010) 21–27

Contents lists available at ScienceDirect

Applied Catalysis B: Environmental

journal homepage: www.elsevier.com/locate/apcatb

Limiting mechanisms in catalytic steam reforming of dimethyl ether

Kajornsak Faungnawakij[a,*], Naohiro Shimoda[b], Nawin Viriya-empikul[a], Ryuji Kikuchi[c], Koichi Eguchi[b]

[a] National Nanotechnology Center (NANOTEC), National Science and Technology Development Agency, 111 Thailand Science Park, Paholyothin Rd., Klonglaung, Patumthani 12120, Thailand
[b] Department of Energy and Hydrocarbon Chemistry, Graduate School of Engineering, Kyoto University, Nishikyo-ku, Kyoto 615-8510, Japan
[c] Department of Chemical System Engineering, School of Engineering, University of Tokyo, 7-3-1 Hongo, Bunkyo-ku, Tokyo 113-8656, Japan

ARTICLE INFO

Article history:
Received 13 November 2009
Received in revised form 3 March 2010
Accepted 6 March 2010
Available online 12 March 2010

Keywords:
Limiting mechanism
Steam reforming
Dimethyl ether
Deactivation
Hydrogen fuel cell

ABSTRACT

The limiting mechanisms in dimethyl ether steam reforming (DME SR) are experimentally investigated over the nanocomposite catalysts of Cu spinel and alumina. The dominant reactions involved in DME SR are proved to be DME hydrolysis to methanol over acidic sites of alumina and subsequent methanol steam reforming to H_2 and CO_2 over Cu sites, followed by reverse-water gas shift reaction. The contribution of other side reactions is also clearly evaluated. DME hydrolysis is limited by the equilibrium, and the hydrolysis rate was much slower than the methanol SR rate, and thus was a rate-determining step in DME SR. The deactivation of Cu spinel was significantly faster than that of alumina, and would determine the lifetime of the composite catalysts. With varied superficial velocities up to 5.2 cm s^{-1} (25 °C, 1 atm), the evidence of mass transfer-limiting mechanism and reaction-limiting mechanism was observed in the low flow rate and the high flow rate regions, respectively.

1. Introduction

Steam reforming (SR) is a method of producing hydrogen from hydrocarbon fuels. It is a distinguished process to produce hydrogen on an industrial scale, and is a current attractive route to provide hydrogen to fuel cells on a small/medium scale. Unlike combustion engine, hydrogen fuel cells generate electricity with only water as a single chemical product and therefore benefit the environment. Using fuel cells can also diminish a dependence on fossil fuels. Some hydrogen sources, e.g. liquefied petroleum gas (LPG), ethanol, methanol (MeOH), and dimethyl ether (DME), have been used in SR [1–4]. Among them, steam reforming of dimethyl ether is currently recognized as a promising process for catalytic hydrogen production [5]. A biomass-derived DME is an oxygenated hydrocarbon without C–C bonds that provides a high hydrogen-to-carbon ratio. It has been used as a clean-burning fuel alternative to LPG and diesel. DME and MeOH are suitable for on-board reforming; they can catalytically be reformed at low temperatures of 200–350 °C for MeOH [6–9] and 200–400 °C for DME [10–15]. DME is harmless and less explosive, and therefore is preferable to MeOH. The utilization of LPG infrastructures to handle DME can be possible due to their similar physical properties, making DME attractive for residential use as well. In addition, autothermal reforming of DME over Pd-based catalysts has also been developed for automobile uses [16].

DME SR ($(CH_3)_2O + 3H_2O_{(g)} \rightarrow 6H_2 + 2CO_2$, $\Delta H_r^0 = 122\ kg\ mol^{-1}$) proceeds via two moderately endothermic reactions in sequence: hydrolysis of DME to MeOH and steam reforming of MeOH to hydrogen and carbon dioxide. Hydrolysis of DME takes place over acid catalysts, e.g. zeolite and alumina, while MeOH SR proceeds over Cu-, Pt-, or Pd-based catalysts. Therefore, bi-functional catalysts containing both acidic and metallic sties are generally needed for DME SR. The Cu-based catalysts are promising in terms of cost effectiveness and activity. We have proposed the Cu-based spinels mixed with γ-Al_2O_3 for DME SR [17–20]. The Cu spinels exhibited excellent performance as compared with Cu/ZnO and Cu/ZnO/Al_2O_3. A sizable number of solid acid catalysts such as H-mordenite, Y-zeolite, and alumina have been proposed as DME hydrolysis catalysts. As compared to strong acids such as H-mordenite and H-ZSM5, γ-alumina possesses relatively weak acid sites and therefore provides lower hydrolysis activity. Nevertheless, a high durability along with inhibition of side reactions was observed from the weak acids [19]. A high temperature above 300 °C is required for effective hydrolysis of DME over γ-Al_2O_3. The high temperature brings about, however, severe sintering of copper [21,22]. Limiting mechanisms in catalytic reaction are the important aspects to understand, design, and develop the catalysts and systems for the reaction processes. There is however no evident report on limiting mechanisms in DME SR so far.

In this work, we explored the limiting mechanisms in DME SR over Cu-based spinel and alumina. The parameters studied were

* Corresponding author. Tel.: +66 2 564 7100x6638; fax: +66 2 564 6981.
E-mail addresses: kajornsak@nanotec.or.th, jiw037@yahoo.com (K. Faungnawakij).

0926-3373/$ – see front matter © 2010 Elsevier B.V. All rights reserved.
doi:10.1016/j.apcatb.2010.03.010

reaction temperature, gas flow rate, and configuration of catalyst bed which strongly affected the catalyst performance and reaction behaviors. The reaction and limiting mechanisms were discussed based on the experimental measurements of structural characteristics and reaction behaviors of the catalyst.

2. Experimental

2.1. Catalyst preparation and characterization

Cu-based spinel used in this work was copper-ferrite spinel oxide ($CuFe_2O_4$) which was prepared by a citric acid complex method as described elsewhere [17,18,23]. The different cations can effectively be accommodated in the complex, providing uniform mixing of the cations [23–26]. An aqueous solution of corresponding nitrates and citric acid was heated to 90 °C to evaporate water until viscous gel was formed. The precipitate obtained was then heated to 140–200 °C until fine powders were achieved. Subsequently the calcination of the powder was conducted in air at 900 °C for 10 h. Gamma-alumina (ALO8) provided by the Catalysis Society of Japan was calcined in air at 700 °C for 0.5 h prior to investigation. The Cu spinel was mechanically mixed with the alumina at a fixed weight ratio of 2:1. The mixture was then pressed, crushed, and sieved to particle sizes of 0.85–1.7 mm. In addition, the Cu spinel and alumina were separately pelletized to the same particle size. For the limiting mechanism tests, the particles were placed randomly or as layers in the reactor.

A nitrogen adsorption system (BEL Japan Bellsorp–max) was employed to determine adsorption–desorption isotherms. The Brunauer–Emmett–Teller (BET) and the Barrett–Joyner–Halenda (BJH) approaches were employed to determine the surface area and pore size distribution of the samples, respectively. The crystalline bulk phase of the catalysts was measured by powder X-ray diffraction (XRD) technique using a Rigaku RINT1400 and a JEOL JDX-3530 with Cu Kα radiation source. The crystallite size was calculated by XRD-line broadening using the Scherrer equation. Scanning electron microscope (SEM, Hitachi S-3400N TypeII) was used to observe morphology of the catalysts. Transmission electron microscope (TEM, Hitachi H-9000UHR III) was used for the observation of microstructure, high resolution TEM image, and diffraction image. Temperature-programmed oxidation (TPO) was employed to analyze the carbon deposition on catalyst surface. A 50 mg catalyst sample was oxidized in 5% O_2/He at a flow rate of 30 ml min^{-1} (25 °C, 1 atm) at a heating rate of 10 °C min^{-1}. The product gases were monitored by online mass spectrometer. X-ray photoelectron spectroscopy (XPS) was performed using a Shimadzu ESCA-850 with a Mg Kα radiation source ($h\upsilon$ = 1253.6 eV) and operated at 8 kV and 30 mA. Each binding energy was referenced to the C 1s peak (284.3 eV).

2.2. Evaluation of catalytic performance

The evaluation of catalytic activity was carried out using a conventional flow reactor under atmospheric pressure. Prior to the evaluation of catalysts, reduction of the catalyst was carried out at 350 °C for 3 h in 10% H_2/N_2. The reaction was attained at each condition for 1 h to achieve a steady state prior to the gas analysis, except in the time-on-stream test. Mass flow controllers were used to adjust the gas feed rate and a low pressure gradient pump to control the water feed rate. A mixture of DME and steam at a steam-to-carbon ratio (S/C) was supplied to a pre-heater at temperature of 150 °C, and then to the catalyst bed at reaction temperature.

The analysis of influent and effluent gaseous compositions was carried out by using online gas chromatographs equipped with a thermal conductivity detector (VARIAN, CP-4900). The steam in the gas stream was trapped by a condenser at ca. 3 °C before the gas analysis. A PoraPLOT Q column was used for the separation of DME, MeOH, and CO_2 and a molecular sieve 5A column for separation of H_2, O_2, N_2, CH_4, and CO. DME conversion and selectivity to gaseous products (S_i) are defined as follows:

$$\text{DME conversion}\,(\%) = 100\left(\frac{F_{CO}+F_{CO_2}+F_{CH_4}+F_{MeOH}}{F_{CO}+F_{CO_2}+F_{CH_4}+F_{MeOH}+2F_{DME}}\right)$$

$$S_i(\%) = 100\left(\frac{F_i}{F_{CO}+F_{CO_2}+F_{CH_4}+F_{H_2}}\right)$$

where F stands for the effluent molar flow rate of each chemical species, and i stands for gaseous products (CO, CO_2, CH_4, or H_2). The deviation of the conversion and the gaseous product distribution (concentration) was typically within ±1% in the duplicated experiments. The reported results were calculated based on the average value obtained by triple gas analyses at each condition.

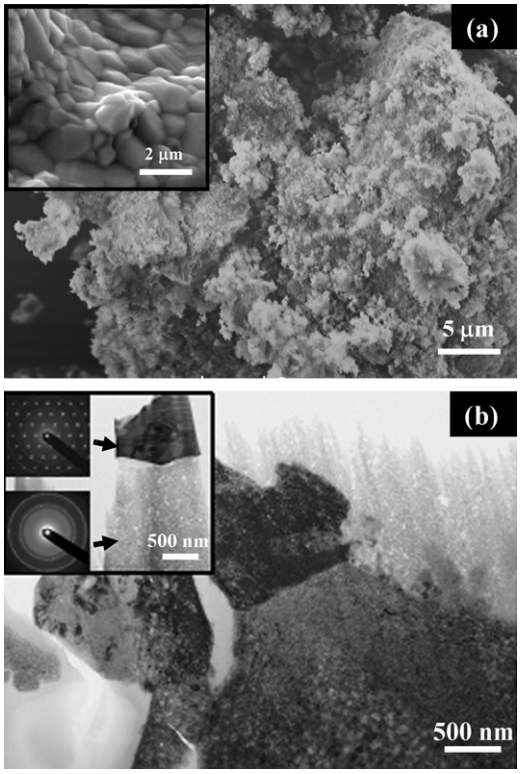

Fig. 1. Typical SEM and TEM micrographs of composite of $CuFe_2O_4$ and Al_2O_3. (a) SEM image with a highly magnified image of $CuFe_2O_4$ (as an inset); (b) TEM image with its zoomed-in image and corresponding SAED (as an inset).

3. Results and discussion

3.1. Characteristics of catalyst

The SEM and TEM images of composite catalyst of $CuFe_2O_4$ and γ-Al_2O_3 are shown in Fig. 1. As seen in Fig. 1(a), the well-mixed state between Cu spinel and alumina was observed in a microscopic scale, while the clean surface of Cu spinel is shown as an inset. The BET surface area of alumina is 141 m^2 g^{-1}, while spinel $CuFe_2O_4$ was a less-porous catalyst with a surface area of 0.5–1 m^2 g^{-1}. The close contact of spinel and alumina is demonstrated in nano-scale by TEM analysis in Fig. 1(b). The SAED images (as an inset) revealed that the Cu spinel is highly crystallized, whereas alumina is almost in amorphous phase. The crystallite size of $CuFe_2O_4$ was ca. 40–45 nm. XRD analysis confirmed that $CuFe_2O_4$ was well crystallized in tetragonal

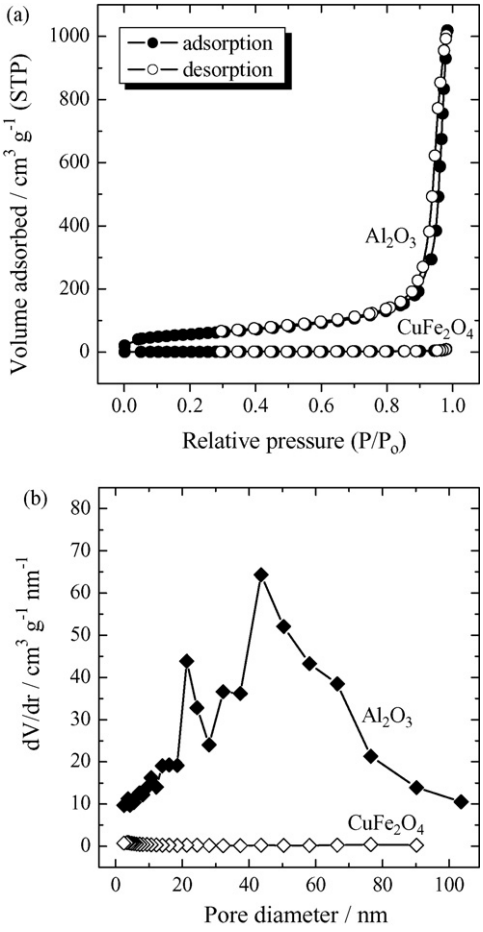

Fig. 2. (a) Nitrogen adsorption–desorption isotherms and (b) BJH pore size distributions of $CuFe_2O_4$ and Al_2O_3.

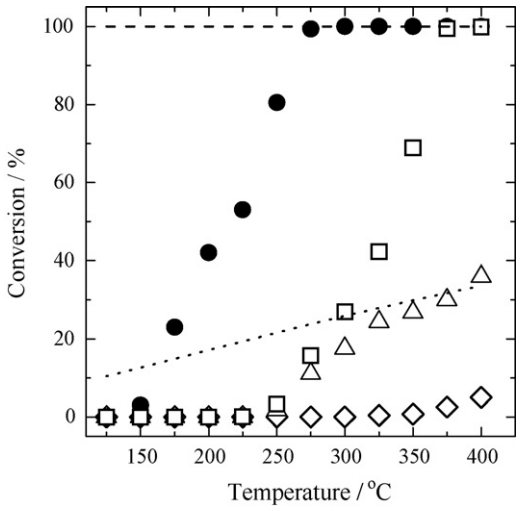

Fig. 3. Temperature dependence of MeOH conversion (●) and DME conversion (□, △, and ◊). Reaction conditions: (●) MeOH SR over $CuFe_2O_4$ at GHSV = 19 000 h^{-1}; S/C = 1.5; catalyst weight = 0.67 g. (□) DME SR over composite of $CuFe_2O_4$ and Al_2O_3 at GHSV = 7000 h^{-1}; S/C = 2; catalyst weight = 1.00 g. (△) DME hydrolysis over Al_2O_3 at GHSV = 11 000 h^{-1}; S/C = 2; catalyst weight = 0.33 g. (◊) DME decomposition over $CuFe_2O_4$ at GHSV = 19 000 h^{-1}; S/C = 2; catalyst weight = 0.67 g. (– – –) the equilibrium conversion of DME in DME hydrolysis, (– – –) the equilibrium conversion of MeOH and DME in SR.

phase, while alumina had low crystallinity in gamma phase, or was in an amorphous form. The dry-mechanical mixing process is an effective and simple way to prepare the composite catalyst. Prior to the reaction, $CuFe_2O_4$ was reduced by hydrogen to form metallic Cu and Fe_3O_4, while γ-Al_2O_3 remained stable under the reduction conditions (results now shown). Even without pre-reduction, $CuFe_2O_4$ could be reduced to metallic Cu and Fe_3O_4 under the working condition via *in situ* activation process [3]. Based on TEM and XRD analyses, after H_2 reduction at 250–350 °C the crystallite size of Cu was ca. 20–25 nm, while that of Fe_3O_4 was ca. 30–35 nm. No evidence of solid solution formation, such as CuFe and CuAl, was observed based on the present results. The Cu species is expected to be a dominant species contributing in MeOH SR.

Based on XPS observation upon reduction/reaction, the majority of chemical state of Cu would be zero- and mono-valent, while that of Fe would be di- and tri-valent. The chemical state of Al was tri-valent (results not shown). The strong chemical interaction between Cu and Fe species was observed to play a crucial role on a high activity and stability of the spinel catalyst as observed by transmission electron microscope and X-ray photoelectron spectroscopy coupled with Auger electron spectroscopy [15,23].

The N_2 adsorption–desorption isotherms and the BJH pore size distribution of the Cu spinel and Al_2O_3 are depicted in Fig. 2. The Cu spinel possessed an extremely low porosity with pore volume below 0.005 ml g^{-1}. The alumina exhibited a type IV isotherm based on IUPAC classification, which was typical of a mesoporous material. As compared with the spinel, the alumina provided a huge adsorption capacity with pore volume of 1.180 ml g^{-1}. The BJH analysis of the highly porous alumina revealed its meso-porous/macroporous structure with a broad pore size distribution from ca. 5 to 100 nm. It should be noted that BET surface area and pore volume of the spinel slightly increased after H_2 reduction or reforming reaction, corresponding to the phase separation of spinel into Cu and Fe_3O_4 during the reduction course. It is worth noting that the alumina possessed a weak acid strength with an acid amount of 50 μmol g^{-1}, whereas the Cu spinel has no acidity.

3.2. Reaction mechanisms and rate-determining step

Fig. 3 shows the catalytic activity of $CuFe_2O_4$, Al_2O_3, and composite of them in DME hydrolysis, MeOH SR, and DME SR. The alumina was active for DME hydrolysis (Reaction (1)) from temperature above 250 °C, and limited at the hydrolysis equilibrium, while hydrolysis activity over Cu spinel was suppressed at extremely low at temperature up to 350 °C. This result revealed that both metallic Cu and Fe_3O_4 could not effectively hydrolyze DME. The activity of Cu spinel for MeOH SR (Reaction (2)) was observed at temperature from ca. 175 °C. The conversion increased monotonously with increasing temperature and reached 100% conversion at 275 °C. The reaction rate of MeOH SR over the Cu spinel is much faster than that of DME hydrolysis over the alumina under the reaction conditions studied. Fig. 4 shows selectivity to CO, CO_2, and H_2 during DME SR over composite catalyst of Cu spinel and alumina. At temperature below 325 °C, CO selectivity was suppressed at essentially zero. H_2 selectivity was obtained at ca. 74.5-75.8%, while CO_2 selectivity was attained at ca. 24.2-25.5%. At temperature above 325 °C, CO selectivity gradually increased to 2.4% at 400 °C, corresponding with the change of selectivities to H_2 and CO_2, presumably due to the contribution of r-WGSR. CH_4 selectivity was trace, suggesting a minor contribution of DME decomposition. Fig. 5 displays concentrations of gaseous reformate produced in DME-steam reaction tests over Cu spinel and alumina. Over alumina, CO_2 formation was suppressed at essentially zero at temperatures up to 375 °C. CO, CH_4, and H_2 were generated at temperatures greater than 350 °C. This result indicated that besides a dominant reaction of DME hydrolysis, DME decomposition (Reaction (4)) partially proceeds over alumina at temperatures above 350 °C and that other side reactions were negligible. In contrast, over $CuFe_2O_4$,

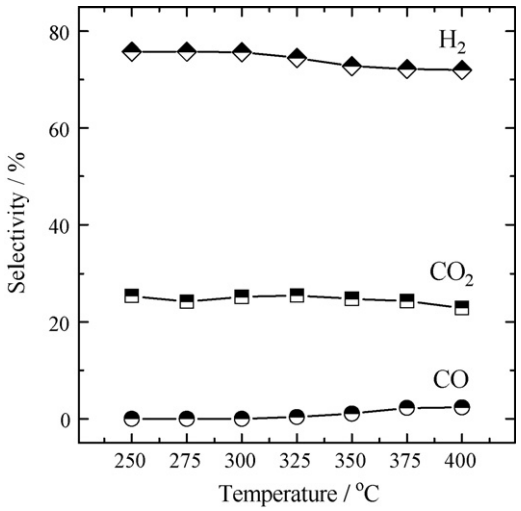

Fig. 4. Temperature dependence of selectivity to CO_2, CO, and H_2 during DME SR over composite of $CuFe_2O_4$ and Al_2O_3. Reaction conditions: GHSV = 7000 h^{-1}; S/C = 2; catalyst weight = 1.00 g.

CO_2 was obviously detected at temperatures from 275 °C, while CO formation was suppressed throughout the temperature range studied. The observed CH_4 and CO_2 accompanied with markedly high production of H_2 suggested an occurrence of a direct route for CO_2 formation from DME and steam (Reaction (5)). The increment of temperature expedited the DME-steam reaction, giving rise to higher H_2, CH_4, and CO_2 formation. However, at temperature below 300 °C H_2 and CO_2 were produced at the ratio of ca. 3:1 without CH_4 formation suggested that a slight amount of DME was hydrolyzed and the resultant MeOH was reformed to H_2 and CO_2. The absence of CO suggested that reverse-water gas shift reaction (r-WGSR) did not significantly proceed over Cu spinel under the present condition studied at the high GHSV and the high S/C ratio. Fukunaga et al. [27] recently proposed with detailed mechanisms that the direct route for CO_2 formation from DME and steam (Reaction (5)) occurred over CuZnAl catalysts at reaction temperature of 400 °C. It should be reminded that over the composite catalysts of Cu spinel and alumina DME hydrolysis followed by MeOH SR are dominant reactions.

$$\text{DME hydrolysis}: \quad (CH_3)_2O + H_2O_{(g)} \rightarrow 2CH_3OH_{(g)}, \quad \Delta H_r^0 = 24\,\text{kJ mol}^{-1} \tag{1}$$

$$\text{MeOH SR}: \quad CH_3OH_{(g)} + H_2O_{(g)} \rightarrow 3H_2 + CO_2, \quad \Delta H_r^0 = 49\,\text{kJ mol}^{-1} \tag{2}$$

$$\text{r-WGSR}: \quad CO_2 + H_2 \rightarrow H_2O_{(g)} + CO, \quad \Delta H_r^0 = 41\,\text{kJ mol}^{-1} \tag{3}$$

$$\text{DME decomposition}: \quad (CH_3)_2O \rightarrow CH_4 + CO + H_2, \quad \Delta H_r^0 = -1\,\text{kJ mol}^{-1} \tag{4}$$

$$\text{Direct } CO_2 \text{ formation}: \quad (CH_3)_2O + H_2O_{(g)} \rightarrow CH_4 + CO_2 + 2H_2, \quad \Delta H_r^0 = -42\,\text{kJ mol}^{-1} \tag{5}$$

Based on the experimental results, a simplified DME SR process over the composite catalyst is schematically shown in Scheme 1. All reactions involved in the reforming process are listed above. The reaction step in DME SR proceeds as follows: DME is first hydrolyzed over acidic sites of alumina to produce MeOH, and

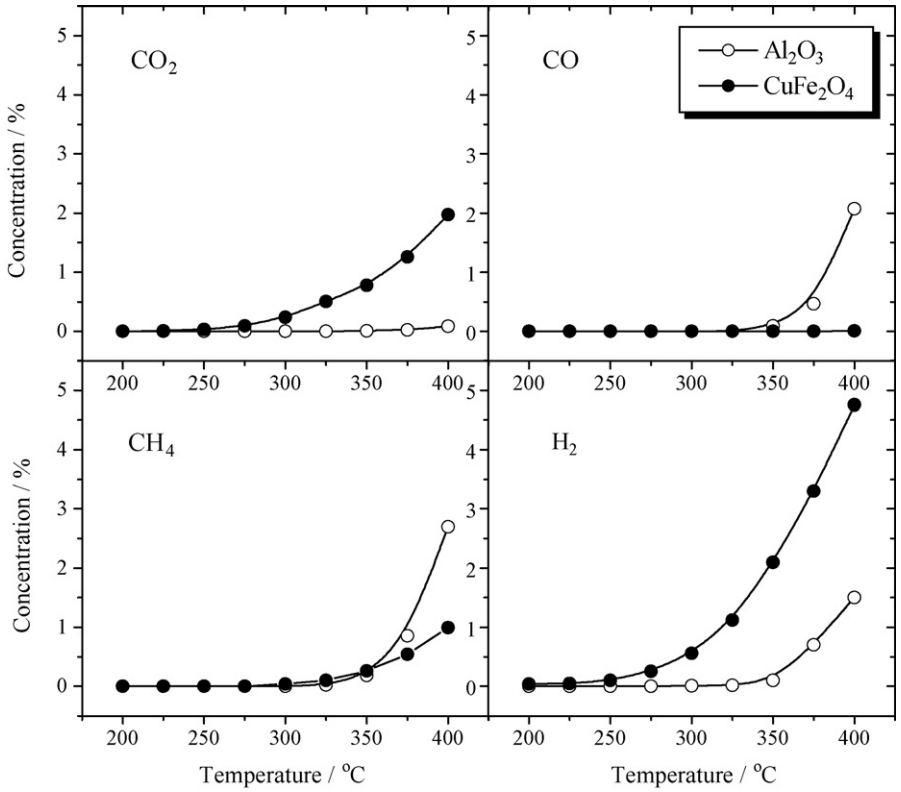

Fig. 5. Temperature dependence of concentration of CO_2, CO, CH_4, and H_2 during DME-steam reaction over $CuFe_2O_4$ and Al_2O_3. Reaction conditions: over Al_2O_3 at GHSV = 11 000 h^{-1}; S/C = 2; catalyst weight = 0.33 g; over $CuFe_2O_4$ at GHSV = 19 000 h^{-1}; S/C = 2; catalyst weight = 0.67 g. Total flow rate was fixed at 100 ml min^{-1}.

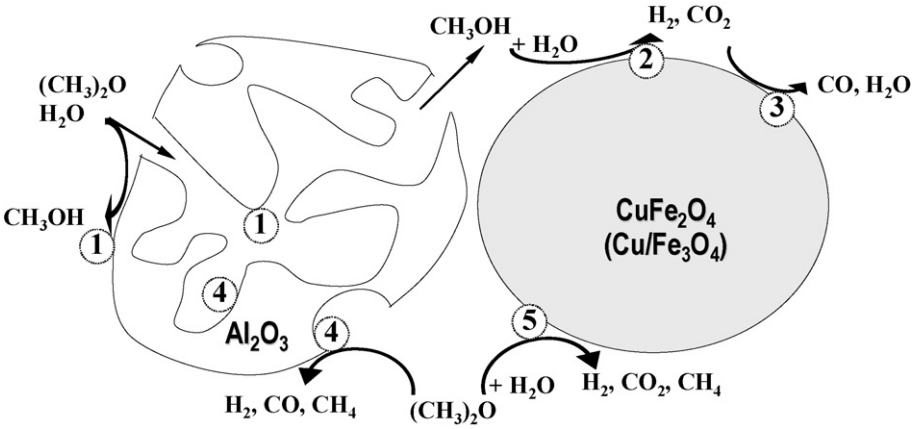

Scheme 1. Simplified reaction mechanism of DME-steam reaction over Cu spinel and alumina.

subsequently MeOH SR proceeds over Cu-based catalysts to form hydrogen and carbon dioxide. Direct decomposition of MeOH to CO and H_2 was known not to be predominantly catalyzed over Cu catalysts [28]. DME hydrolysis over alumina and MeOH SR as well as r-WGSR over Cu spinel are highly selective and dominant in the present reforming system, while other side reactions are very minor. Although DME hydrolysis is reversible and controlled by thermodynamic equilibrium, MeOH produced from DME is continuously converted by MeOH SR reaction, which is fast enough and thus expected to attain complete conversion of MeOH under the current experiments. Consequently, DME would be completely converted over the composite of Cu spinel and alumina. Since DME SR proceeds via the 2-step reaction, a close contact between acidic sites of Al_2O_3 and active sites of Cu spinel is highly requisite. By this way, MeOH produced via DME hydrolysis is expected to be instantly reformed to H_2 and CO_2, leading to high overall DME conversion. Since Al_2O_3 is highly porous, both external diffusion on the surface and internal diffusion in the alumina pores of DME and steam would play a role in the hydrolysis step. A minority of side reactions of DME decomposition to H_2, CH_4, CO_2, and CO over alumina and $CuFe_2O_4$ in the presence of water is initiated at temperature of ca. 350 °C. The results also suggested that decomposition of DME and MeOH are negligible over Fe_3O_4 at temperatures below 350 °C.

3.3. *Effect of configuration of catalyst bed and stability test*

DME SR was carried out in catalyst beds of different configurations to examine the effect of the bed configuration on the catalytic performance. Three configurations of the bed were set by placing pelletized samples of Cu spinel, alumina, or composite of them as in the following manner: (1) packed bed of well-mixed composite, (2) packed bed of alumina and Cu spinel pellets placed randomly, and (3) packed bed of four layers of alumina and Cu spinel placed alternatively, as displayed in Fig. 6. As a result, the greatest conversion was achieved over the well-mixed composite. The decrease in the conversion was found when the alumina and the spinel were packed separately (configuration 2) and as layers (configuration 3), respectively. Without mixing, MeOH SR over Cu spinel could not proceed efficiently after DME hydrolysis over alumina. Interparticle diffusion between the alumina and the Cu spinel particles greatly contributed to the reaction. These results confirmed that the mixing state of Cu spinel and alumina was a significant factor for achieving an excellent performance in DME SR. The stability test for Cu spinel and alumina in DME SR was carried out for 1000 h at 375 °C. To clearly figure out which catalyst component of the composite is deactivated during the reaction, the configuration 3 was used for the test. As a result shown in Fig. 7, DME conversion could be attained at 52–55% for 800 h, but continuously dropped to ca. 40% at 1000 h. Although the spent alumina was replaced by the fresh one, the conversion could not be recovered to the original level and continued to decline. On the contrary, the conversion was efficiently recovered after the replacement of the spent Cu spinel by the fresh one. Nevertheless, the recovered activity was still slightly lower than the initial activity, indicating that the alumina was also partly degraded. These results revealed that the deactivation of Cu spinel was much faster than that of the alumina and that deactivation of the composite would stem mainly from that of Cu spinel. The Cu crystallite size of the spent spinel was calculated using the Scherrer formula at the respective Cu[1 1 1] reflections, and it was found that the crystallite size increased from ca. 24–25 to 32–33 nm after reaction time of 1000 h, confirming the sintering effect. After the reaction test, no evidence for carbon deposition on either the alumina or the Cu spinel surfaces was quantitatively observed by TPO analysis, though we previously observed that coking also par-

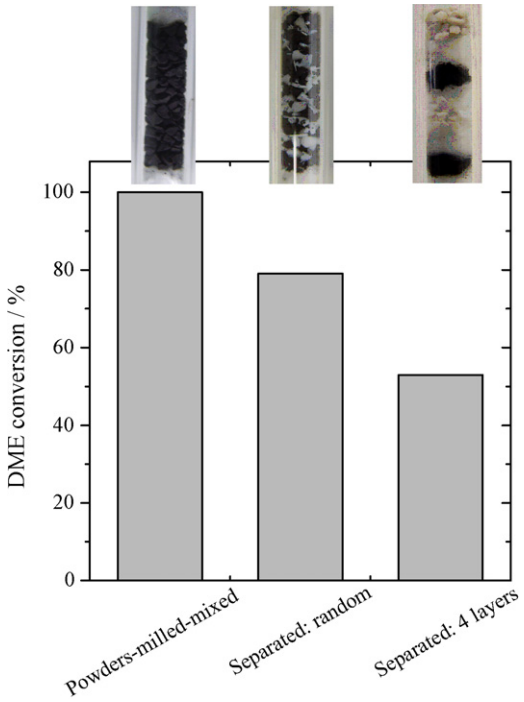

Fig. 6. Effect of configuration of catalyst bed on DME SR activity. Reaction conditions: GHSV = 4000 h^{-1}; S/C = 2.5; catalyst weight = 0.6 g (0.2 g alumina and 0.4 g Cu spinel).

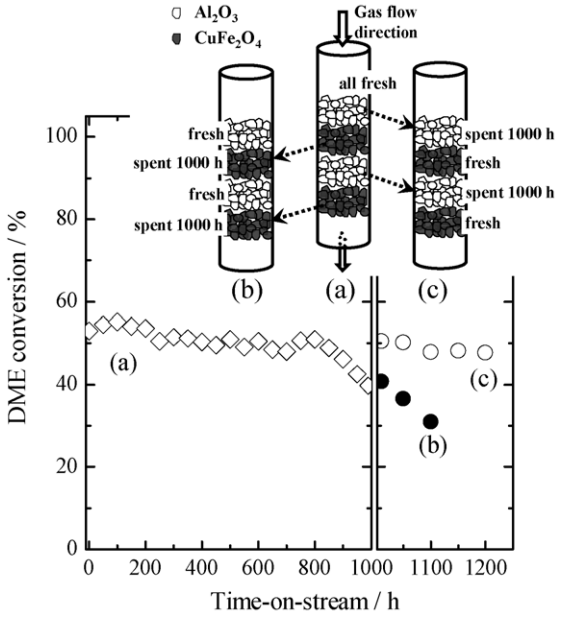

Fig. 7. Stability test of the spinel and alumina in DME SR. Reaction conditions: GHSV = 4000 h^{-1}; S/C = 2.5; catalyst weight = 0.6 g (0.2 g alumina and 0.4 g Cu spinel).

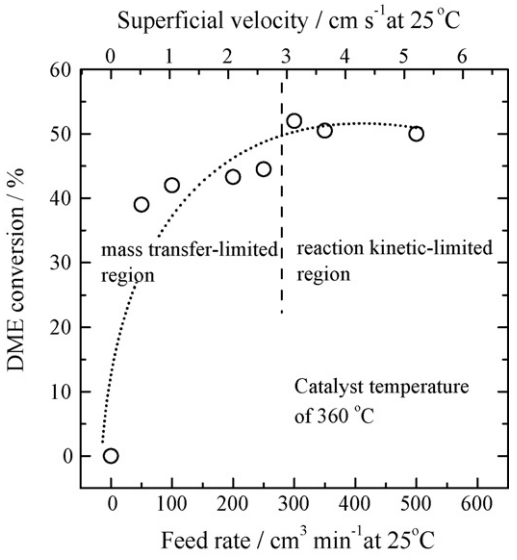

Fig. 8. Limiting mechanisms in DME SR over composites of $CuFe_2O_4$ and Al_2O_3: DME conversion *vs* feed flow rate. Reaction conditions: S/C = 2.5; GHSV = 15 000 h^{-1}.

tially contributed to degradation of the heat-treated composite catalysts after 1100 h test [4]. It was reported that carbonaceous deposition significantly occurred in DME SR over Cu-based catalyst mixed with strong acids such as WO_3/ZrO_2 and ZSM-5 [29,30]. On the other hand, coking over alumina-based composite catalyst was relatively low [19,31]. Doping of Ni species to Cu–Fe spinel was recently proposed to promote the stability of the catalysts owing to the nano-alloy formation [32].

3.4. Limiting mechanisms

Limiting mechanisms in steam reforming process were studied in this section. Generally, mass transfer, heat transfer, chemical kinetics, and/or chemical thermodynamic equilibrium are considered to be dominant limitations in catalytic reactions. A thermodynamic equilibrium analysis shows that DME SR is not controlled by chemical reaction equilibria [33]. Although hydrolysis of DME to MeOH is equilibrium-controlled at relatively low conversions, MeOH can be continuously converted by MeOH SR and consequently complete conversion of DME can be obtained over the composite catalysts. We confirmed that the mixing ratio between Cu spinel and alumina at 2-to-1 provided sufficient amounts of acid and copper sites to achieve complete conversion of DME at reaction temperatures above 300 °C [19].

A mass transfer-limiting mechanism was evaluated by measuring DME conversion at varied feed flow rates up to 500 ml min^{-1} (corresponding to superficial velocity of 5.2 m s^{-1} at 25 °C) at a fixed GHSV of 15 000 h^{-1}. The catalyst temperature was fixed at 360 °C, so that heat transfer limitation could be neglected. As shown in Fig. 8, the conversion increased with increasing flow rate up to ca. 300 ml min^{-1}, and then leveled off. The region where the reaction rate is dependent of the velocity of fluid can be defined as a mass transfer-limited region. Above the mass transfer-limited region, the rate of reaction is no longer limited by the mass transfer at high flow rates—this region is known as a reaction-limited region [34]. This chemical kinetics-controlled reaction occurs when mass transfer rate of reactants to active sites is faster than the kinetic reaction rate. Operating the reforming reaction beyond mass-transfer limitation leads to a high activity, especially when in a high conversion region in which DME concentration gradient between bulk and catalyst surface are extremely low. It was considered that the mass transfer limitation, especially the intraparticle diffusion in a porous alumina catalyst and the interparticle diffusion between the alumina and Cu spinel catalysts played a significant role in limiting the overall reaction rate (as depicted in Fig. 5).

We proposed a new approach to investigate the limiting mechanism in DME SR by measuring catalyst temperature profiles along the catalyst bed with varied feed flow rates. The reaction rate was monitored by means of catalyst temperature, since the higher degree of reaction gives rise to higher endothermicity, resulting in a lower catalyst temperature. A typical axial profile of catalyst temperature measured locally along the axis of the reactor is shown in Fig. 9. At a fixed setpoint temperature, under N_2 flow the catalyst temperature at each measurement point remained essentially constant along the bed at 375 °C. When a mixture of DME and steam was fed to the bed at a flow rate of 50 ml min^{-1}, the catalyst temperature obviously dropped to ca. 367 °C at the inlet of the catalyst bed, and increased along the flow direction, up to 375 °C at the end. The higher feed rate would result in more steep decrease in catalyst temperature in the vicinity of the reactor inlet. The catalyst temperatures at the beginning of the bed (0–0.5 cm), where only reforming

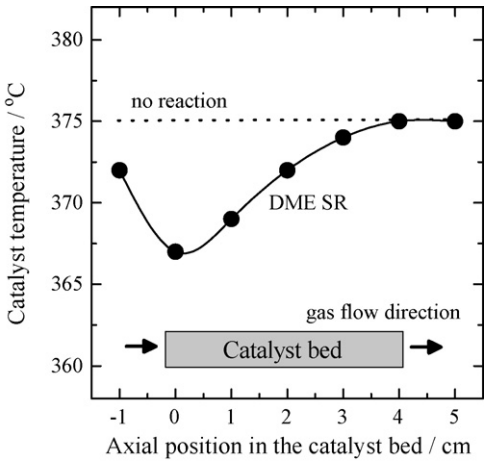

Fig. 9. Typical axial temperature profile along the catalyst bed. Reaction conditions: GHSV = 500 h^{-1}; S/C = 2.5.

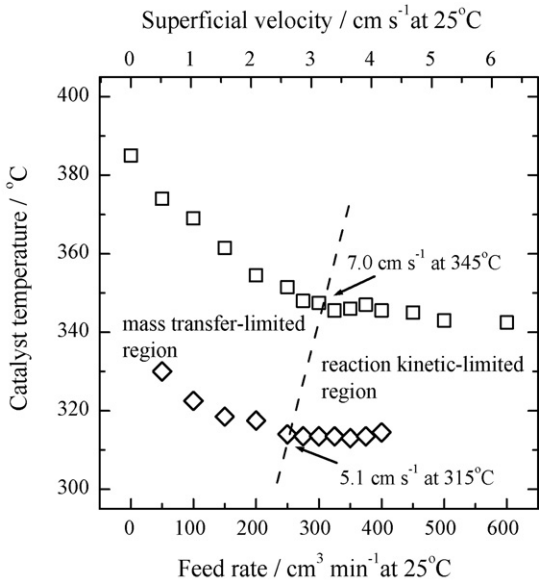

Fig. 10. Limiting mechanisms in DME SR over composites of $CuFe_2O_4$ and Al_2O_3: catalyst temperature *vs* feed flow rate. Reaction conditions: S/C = 2.5; the catalyst temperatures were taken from the inlet zone of catalyst bed (0–0.5 cm).

reaction is considered to solely take place, were representatively used as an indicator of the reaction rate. In Fig. 10 the catalyst temperatures are depicted as a function of feed flow rate and superficial velocity. The higher feed rate up to ca. 250–300 $cm^3\ min^{-1}$ gives rise to lower the catalyst temperature due to the higher degree of endothermic reactions. Further increase in the feed rate could not lower the catalyst temperature. The stable catalyst temperature is ascribable to the constant extent of the reaction which is known to be controlled by the kinetic rate. The minimum superficial velocity to avoid mass transfer limitation is determined as 7.0 and 5.1 cm s^{-1} for catalyst temperature of 345 and 315 °C, respectively. The lower velocity found at a lower catalyst temperature should be ascribable to the lower kinetic reaction rate. The limiting-mechanism studies shown in Figs. 8 and 10 were consistent well with each other. The behavior of catalyst temperature would be a convenient approach to evaluate the limiting regions in reactions with moderate to high endothermic or exothermic natures.

4. Conclusions

The limiting mechanisms in DME SR were experimentally investigated over Cu spinel and alumina catalysts. The concluding remarks are drawn as follows:

I. The dominant reactions involved in DME SR were DME hydrolysis to MeOH over alumina followed by MeOH SR to H_2 and CO_2, and subsequent r-WGSR over Cu sites. Direct DME decomposition to CH_4, CO, and H_2 over alumina and the direct route for CO_2, CH_4, and H_2 formation from DME-steam reaction over the copper catalyst were very minor.
II. DME hydrolysis rate over the alumina was much slower than MeOH SR rate over the Cu spinel, and was limited by the equilibrium, and was a rate-determining step in DME SR.
III. The deactivation of Cu spinel was significantly faster that that of alumina, and would determine the lifetime of the composite catalysts.
IV. Within the range of superficial velocities up to 5.2 cm s^{-1} (25 °C, 1 atm), the evidence of mass transfer-limiting mechanism and reaction-limiting mechanism were obtained in the low flow rate and the high flow rate regions, respectively.
V. The limiting mechanisms in DME SR were successfully evaluated by two approaches: (i) DME conversion and (ii) local catalyst temperature as the indicator.

Acknowledgements

Authors acknowledge the NANOTEC, the Thailand Research Fund (TRF), and the Japan Science and Technology Agency (JST) for financial supports. Authors thank Dr. Tetsuya Fukunaga from Idemitsu Kosan Co., Ltd., Japan and Prof. Dr. Wiwut Tanthapanichakoon from Chulalongkorn University, Thailand for technical supports.

References

[1] J. Kugai, V. Subramani, C. Song, M.H. Engelhard, Y. Chin, J. Catal. 238 (2006) 430.
[2] N. Laosiripojana, S. Assabumrungrat, J. Power Sources 158 (2006) 1348.
[3] K. Faungnawakij, T. Fukunaga, R. Kikuchi, K. Eguchi, J. Catal. 256 (2008) 37.
[4] M. Turco, C. Cammarano, G. Bagnasco, E. Moretti, L. Storaro, A. Talon, M. Lenarda, Appl. Catal. B 91 (2009) 101.
[5] T.A. Semelsberger, R.L. Borup, H.L. Greene, J. Power Sources 156 (2006) 497.
[6] E.S. Ranganathan, S.K. Bej, L.T. Thompson, Appl. Catal. A 289 (2005) 153.
[7] K. Nishida, I. Atake, D. Li, T. Shishido, Y. Oumi, T. Sano, K. Takehira, Appl. Catal. A 337 (2008) 48.
[8] P. Tolmacsov, A. Gazsi, F. Solymosi, Appl. Catal. A 362 (2009) 58.
[9] G. Avgouropoulos, J. Papavasiliou, M.K. Daletou, J.K. Kallitsis, T. Ioannides, S. Neophytides, Appl. Catal. B 90 (2009) 628.
[10] V.V. Galvita, G.L. Semin, V.D. Belyaev, T.M. Yurieva, V.A. Sobyanin, Appl. Catal. A 216 (2001) 85.
[11] K. Takeishi, H. Suzuki, Appl. Catal. A 260 (2004) 111.
[12] T. Matsumoto, T. Nishiguchi, H. Kanai, K. Utani, Y. Matsumura, S. Imamura, Appl. Catal. A 276 (2004) 267.
[13] Y. Tanaka, R. Kikuchi, T. Takeguchi, K. Eguchi, Appl. Catal. B 57 (2005) 211.
[14] D. Feng, Y. Wang, D. Wang, J. Wang, Chem. Eng. J. 146 (2009) 477.
[15] K. Faungnawakij, N. Shimoda, T. Fukunaga, R. Kikuchi, K. Eguchi, Appl. Catal. B 92 (2009) 341.
[16] M. Nilsson, P. Jozsa, L.J. Pettersson, Appl. Catal. B 76 (2007) 42.
[17] K. Faungnawakij, R. Kikuchi, K. Eguchi, Scripta Mater. 60 (2009) 655.
[18] K. Faungnawakij, N. Shimoda, T. Fukunaga, R. Kikuchi, K. Eguchi, Appl. Catal. A 341 (2008) 139.
[19] K. Faungnawakij, R. Kikuchi, T. Matsui, T. Fukunaga, K. Eguchi, Appl. Catal. A 333 (2007) 114.
[20] K. Faungnawakij, R. Kikuchi, N. Shimoda, T. Fukunaga, K. Eguchi, Angew. Chem. Int. Ed. 47 (2008) 9314.
[21] O. Ilinich, W. Ruettinger, X. Liu, R. Farrauto, J. Catal. 247 (2007) 112.
[22] L. Lloyd, D.E. Ridler, M.V. Twigg, in: M.V. Twingg (Ed.), Catalyst Handbook, second ed., Wolfe Publishing, Frome, 1989, p. 283.
[23] K. Eguchi, N. Shimoda, K. Faungnawakij, T. Matsui, R. Kikuchi, S. Kawashima, Appl. Catal. B 80 (2008) 156.
[24] N. Shimoda, K. Faungnawakij, R. Kikuchi, T. Fukunaga, K. Eguchi, Appl. Catal. A 365 (2009) 71.
[25] U. Zavyalova, B. Nigrovski, K. Pollok, F. Langenhorst, B. Müller, P. Scholz, B. Ondruschka, Appl. Catal. B 83 (2008) 221.
[26] S. Rousseau, S. Loridant, P. Delichere, A. Boreave, J.P. Deloume, P. Vernoux, Appl. Catal. B 88 (2009) 438.
[27] T. Fukunaga, N. Ryumon, S. Shimazu, Appl. Catal. A 348 (2008) 193.
[28] N. Takezawa, N. Iwasa, Catal. Today 36 (1997) 45.
[29] T. Nishiguchi, K. Oka, T. Matsumoto, H. Kanai, K. Utani, S. Imamura, Appl. Catal. A 301 (2006) 66.
[30] T. Kawabata, H. Matsuoka, T. Shishido, D. Li, Y. Tian, T. Sano, K. Takehira, Appl. Catal. A 308 (2006) 82.
[31] F. Solymosi, R. Barthos, A. Kecskemeti, Appl. Catal. A 350 (2008) 30.
[32] K. Faungnawakij, T. Fukunaga, R. Kikuchi, K. Eguchi, J. Phys. Chem. C 113 (2009) 18455.
[33] K. Faungnawakij, R. Kikuchi, K. Eguchi, J. Power Sources 164 (2007) 73.
[34] H.S. Fogler, Elements of Chemical Reaction Engineering, third ed., Prentice-Hall International Inc., New Jersey, 1999.